environments

MDPI

Article

Iron Oxide Nanoparticles for Photosynthetic Recovery in Iron-Deficient 'Micro-Tom' Tomato Plants

João Pedro Sampaio Gama [1], Felipe Girotto Campos [1,*], Carla dos Santos Riccardi [2] and Carmen Sílvia Fernandes Boaro [1]

[1] Department of Biodiversity and Biostatistics, Institute of Biosciences, São Paulo State University—UNESP, Botucatu 18618-689, Brazil; joao.gama@unesp.br (J.P.S.G.); carmen.boaro@unesp.br (C.S.F.B.)
[2] Department of Bioprocesses and Biotechnology, School of Agricultural Sciences, São Paulo State University—UNESP, Botucatu 18610-034, Brazil; carla.riccardi@unesp.br
* Correspondence: felipe.girotto@unesp.br

Abstract

In plant tissues, nanoparticles can stimulate the production of reactive oxygen species (ROS), which, in excess, cause cellular toxicity by damaging membranes, chloroplasts, and DNA. However, they can also activate antioxidant mechanisms, aiding metabolic recovery under oxidative stress. In agriculture, iron oxide (nFe) nanoparticles stand out for their gradual release of the nutrient, preventing leaching and increasing productivity. This study aims to investigate whether iron oxide nanoparticles are effective alternatives for overcoming iron deficiencies, mitigating oxidative stress and restoring metabolic functions, while maintaining photosynthesis. The high H_2O_2 concentration observed in nFe 500 mg L^{-1} (nFe 500) suggests that Fe, after being transported by the nanoparticles to the leaves, may have acted as a cofactor for antioxidant enzymes involved in H_2O_2 decomposition, reducing malondialdehyde concentration (MDA). Maintaining low oxidative stress suggests that H_2O_2 may function not only as a stress indicator but also as a signaling molecule in intracellular processes. nFe 500 suggests the ability of plants to utilize released Fe^{2+}/Fe^{3+}, restoring photosynthetic function in iron-deficient plants.

Keywords: magnetite nanoparticles; chlorophyll *a* fluorescence; gas exchange; oxidative stress; *Solanum lycopersicum*

check for updates

Academic Editor: Gabriel Gascó Guerrero

Received: 6 August 2025
Revised: 11 September 2025
Accepted: 24 September 2025
Published: 26 September 2025

Citation: Gama, J.P.S.; Campos, F.G.; Riccardi, C.d.S.; Boaro, C.S.F. Iron Oxide Nanoparticles for Photosynthetic Recovery in Iron-Deficient 'Micro-Tom' Tomato Plants. *Environments* **2025**, *12*, 346. https://doi.org/10.3390/environments12100346

Copyright: © 2025 by the authors. Licensee MDPI, Basel, Switzerland. This article is an open access article distributed under the terms and conditions of the Creative Commons Attribution (CC BY) license (https://creativecommons.org/licenses/by/4.0/).

1. Introduction

Nanoscience is a rapidly expanding field that has transformed several areas of knowledge by enabling the manipulation of matter at the nanometric scale. At this dimension, materials exhibit unprecedented properties, allowing for innovative applications, such as forest-derived nanocellulose, which reduces the carbon footprint of petroleum-based products, and nanofilters capable of making water potable by removing contaminants. In botany, nanofertilizers are particularly noteworthy. They are composed of nanoparticles of macro- and micronutrients that are released slowly, preventing leaching and enhancing crop production, thus demonstrating the potential of nanoscience to promote sustainable advances [1–3].

Nanoparticles are materials with dimensions ranging from 1 to 100 nanometers. They may occur naturally, being found in atmospheric dust, volcanic eruptions, or resulting from the weathering of igneous rocks, but they can also be generated by human activities, such as by-products of aluminum production or in leachates from landfills. They can be synthesized

from a wide variety of materials, including metals, metal oxides, and carbon, acquiring distinct catalytic, electronic, magnetic, and optical properties due to their reduced size and structural diversity. These characteristics enable the application of nanoparticles across multiple sectors, including industry, electronics, food, and technology, among others [4–7].

The interaction between nanoparticles and plants occurs through leaves or roots and is influenced by their size and chemical composition. Foliar absorption may occur through the cuticle, via lipophilic and hydrophilic channels, or through stomata, depending on the species' anatomy. In roots, fissures in the plasma membrane, caused by mechanical damage, soil herbivores, or microorganisms, represent additional entry routes for nanoparticles [8,9].

Within plant tissues, nanoparticles can stimulate the production of reactive oxygen species (ROS), whose excess is the first sign of cellular toxicity. This imbalance disrupts metabolism, leading to plasma membrane degradation, tissue necrosis, and damage to chloroplasts and DNA. On the other hand, studies indicate that the presence of nanoparticles can also activate the antioxidant system, supporting recovery from oxidative stress. An example is cadmium sulfate nanoparticles, which induce ROS overproduction in the roots of Vicia faba L., thereby signaling the synthesis of glutathione, a key molecule in mitigating oxidative stress [10–13].

In agriculture, nanoparticles are employed with the aim of improving crop quality and yield. Singh et al. [14] reviewed studies confirming that the application of nanofertilizers can increase the bioavailability of mineral nutrients, consequently contributing to higher photosynthetic rates. Among nanoparticles used in agriculture, those synthesized from iron, such as magnetite (Fe_3O_4) and hematite (Fe_2O_3), are particularly relevant, as they may exert both positive and negative effects depending on the applied concentration. Studies have reported that low concentrations of hematite nanoparticles promote increases in chlorophyll production and root elongation in different plant species. Conversely, high concentrations of iron nanoparticles may compromise cellular structures, as observed in studies reporting deformities and damage to the vascular bundles of pepper species [15–18]. Therefore, studies using different concentrations of iron oxide nanoparticles are essential to better understand their implications for plant metabolism.

Based on this context, we hypothesize that in iron-deficient plants, the supply of iron oxide nanoparticles may compensate for the lack of this micronutrient, reestablishing the metabolic functions in which it participates and controlling oxidative stress, thereby supporting their potential application in agriculture. The objective of this study was to investigate oxidative stress and the recovery of photosynthetic parameters in plants supplied with iron oxide nanoparticles through the roots.

2. Materials and Methods

2.1. Experimental Condition

The experiment was conducted in a growth chamber at 27 ± 3 °C, with light radiation of 350 ± 20 µmol m^{-2} s^{-1} and relative humidity of 45 ± 3%, between January and March 2024. All evaluations were performed at the Growth Laboratory of the Department of Biodiversity and Biostatistics, Institute of Biosciences, São Paulo State University (UNESP), Botucatu Campus, São Paulo, Brazil (22°49′10″ S, 48°24′35″ W; average altitude of 800 m).

2.2. Plant Species

Tomato (*Solanum lycopersicum* L. cv. 'Micro-Tom') is one of the most widely cultivated plants and a well-established model species worldwide. Scientific interest in this cultivar arises from the relationship between productivity and responses to biotic or abiotic stress. 'Micro-Tom' was originally developed by crossing the Florida Basket and Ohio 4013-3

cultivars for ornamental purposes. However, traits such as small size, rapid growth, and ease of mutant generation led to its establishment as a convenient research model [19,20].

2.3. Preparation and Functionalization of Iron Oxide Nanoparticles

Magnetite nanoparticles were synthesized at the Central Laboratory of the Faculty of Agricultural Sciences, UNESP, Botucatu Campus. The synthesis involved dissolving 1.405 g of $FeSO_4 \cdot 7H_2O$ in 5.0 mL of H_2O, 2.755 g of $FeCl_3$ in 10.0 mL of H_2O, and 2.0 g of NaOH in 20.0 mL of H_2O. The NaOH solution was slowly added dropwise to the iron salt solution under constant stirring for 15 min to ensure homogeneous dispersion and controlled growth of magnetite nanoparticles. The resulting suspension was allowed to cool to room temperature, and the solid precipitate was repeatedly washed until the rinse water reached neutral pH (7.0). The solid was then washed three times with distilled water to remove non-reactive residues. The precipitate was resuspended in acetone and centrifuged three times at 8000 rpm for 10 min. Finally, the precipitate was dried in a desiccator connected to a DIA-PUMP® air compressor/vacuum system (FANEM, São Paulo, Brazil) at 500 mmHg vacuum pressure and room temperature for 72 h.

2.4. Functionalization of Iron Oxide Nanoparticles

For functionalization, processes were carried out under a nitrogen atmosphere to prevent magnetite oxidation, using citric acid ($C_6H_8O_7$) as the functionalizing agent. A total of 0.2 mg of citric acid was dissolved in 1.0 mL of degassed ultrapure water, after which 1.0 g of iron nanoparticles was sonicated in degassed ultrapure water for 10 min. The citric acid solution was added to the magnetite suspension and stirred vigorously with a mechanical stirrer for 30 min at 80 °C. The suspension was then washed repeatedly with water until the pH of the wash water equaled that of ultrapure water.

2.5. Treatment Application and Experimental Design

Tomato seeds were germinated in four rigid seedling trays, each containing 162 cells with a volume of 31 cm^3 per cell, filled with medium-textured vermiculite. The seedlings remained in these trays until the emergence of the first true leaves (30 days). Subsequently, plants were selected and transplanted into 7.2 dm^3 containers filled with Hoagland and Arnon nutrient solution No. 2 [21] (50% ionic strength), without Fe-EDTA. After 30 days under hydroponic conditions, plants were subjected to six treatments: (1) No-Fe—Hoagland and Arnon solution No. 2, without Fe-EDTA and without iron nanoparticles; (2) nFe (iron oxide nanoparticles) 125—Hoagland and Arnon solution No. 2, without Fe-EDTA, with 125 mg L^{-1} iron oxide nanoparticles; (3) nFe 250—same solution, with 250 mg L^{-1} iron oxide nanoparticles; (4) nFe 500—same solution, with 500 mg L^{-1} iron oxide nanoparticles; (5) Citric Acid (CA)—complete Hoagland and Arnon solution No. 2, without Fe-EDTA, with 1.4704 g L^{-1} citric acid and no iron oxide nanoparticles; (6) Control—complete Hoagland and Arnon solution No. 2, with Fe-EDTA and no iron oxide nanoparticles (Table S1). The experiment was conducted for 21 days, with evaluations at 7, 14, and 21 days after treatment application. Iron-deficient plants did not survive beyond 21 days, as they had already been cultivated for 30 days under iron deficiency. The experiment followed a completely randomized design with six treatments and eight replicates.

2.6. Chlorophyll a Fluorescence and Gas Exchange

Measurements were conducted between 9:00 and 11:00 a.m. under artificial light at an intensity of 200 ± 20 µmol m^{-2} s^{-1}, using the second or third fully expanded leaf. Gas exchange parameters were measured with an infrared gas analyzer (IRGA, GSF 3000, Walz, Effeltrich, Germany) under saturating irradiance of 1200 µmol m^{-2} s^{-1}, coupled to a portable modulated light fluorometer (LED-ARRAY/PAM-Module 3055-FL, Walz, Effeltrich, Germany). For chlorophyll *a* fluorescence analysis, leaves were dark-adapted for 30 min, after which an actinic light pulse of 4500 µmol m^{-2} s^{-1} was applied to determine maximum dark-adapted fluorescence (Fm). Additional parameters included minimum dark-adapted fluorescence (F_0), maximum potential quantum efficiency of PSII (Fv/Fm), effective quantum efficiency of PSII (Fv′/Fm′), electron transport rate (ETR), effective quantum yield of PSII (ΦPSII), photochemical quenching (qP), non-photochemical quenching (NPQ), heat dissipation in the antenna complex (*D*), and excess energy not dissipated or used in photochemistry (*Ex*). Gas exchange parameters measured included transpiration rate (*E*, mmol m^{-2} s^{-1}), stomatal conductance (*gs*, mmol m^{-2} s^{-1}), net carbon assimilation (*A*, µmol m^{-2} s^{-1}), and internal CO_2 concentration (C_i, µmol mol^{-1}). These were calculated using the IRGA's integrated analysis software (Microsoft® Excel® for Microsoft 365 MSO (Version 2508 Build 16.0.19127.20192), based on the general gas exchange equation by von Caemmerer and Farquhar [22]. Instantaneous water-use efficiency (iWUE, µmol CO_2 mmol H_2O^{-1}) was determined as the ratio of net CO_2 assimilation to transpiration. Carboxylation efficiency (A/C_i, µmol m^{-2} s^{-1} Pa^{-1}) was calculated as the ratio of net assimilation to internal CO_2 concentration.

2.7. Quantification of Hydrogen Peroxide

Hydrogen peroxide was quantified according to Alexieva et al. [23], using trichloroacetic acid (TCA) to determine H_2O_2 content in 100 mg of leaves collected and stored in liquid nitrogen at −20 °C. Absorbance was measured at 390 nm with a spectrophotometer, and results were expressed as µmol H_2O_2 g^{-1} fresh weight.

2.8. Lipid Peroxidation

Lipid peroxidation was assessed following Teisseire and Guy [24], using thiobarbituric acid (TBA) and TCA to determine malondialdehyde concentration (MDA) in 100 mg of leaves collected and stored in liquid nitrogen at −20 °C. Absorbance was measured at 560 and 600 nm, and results were expressed as nmol malondialdehyde g^{-1} fresh weight.

2.9. Statistical Evaluation

Data were subjected to analysis of variance (ANOVA). Homogeneity was tested using Levene's test, and means were compared by Tukey's test at a 5% probability level (Tables S2–S4). Statistical analyses were performed with AgroEstat software version 1.1.0.712.

2.10. Heatmap

The heatmap was generated using MetaboAnalyst® v5.0 (Québec, QC, Canada; https://www.metaboanalyst.ca/) (accessed on 30 April 2025) to establish clusters and relationships between treatments and the analyzed variables for different concentrations of iron nanoparticles [25].

3. Results

Figure 1 shows *Solanum lycopersicum* seedlings after 21 days of cultivation under the different treatments.

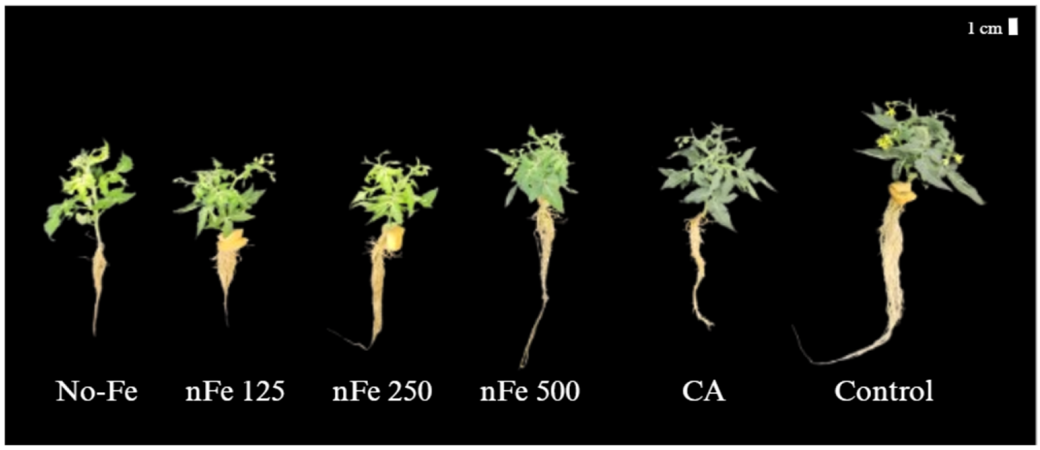

Figure 1. Tomato seedlings (*Solanum lycopersicum* L. cv. 'Micro-tom') at 21 days of cultivation without iron (No-Fe); 125 mg L^{-1}, 250 mg L^{-1} and 500 mg L^{-1} of iron oxide nanoparticles (nFe 125, 250 and 500); 1.47 g L^{-1} of citric acid (CA) and Control with 1.5 mg L^{-1} FeEDTA supplied via 50% Hoagland and Arnon nutrient solution.

3.1. Chlorophyll a Fluorescence

The maximum potential quantum efficiency of PSII (Fv/Fm) was reduced in the No-Fe and nFe 250 treatments. In contrast, the nFe 500 and CA treatments showed similar values (Figure 2A). The nFe 250, nFe 500, and CA treatments displayed higher non-photochemical quenching (NPQ), suggesting increased dissipation of excess energy (Figure 2B). The No-Fe treatment exhibited a higher value of minimum dark-adapted fluorescence (F_0).

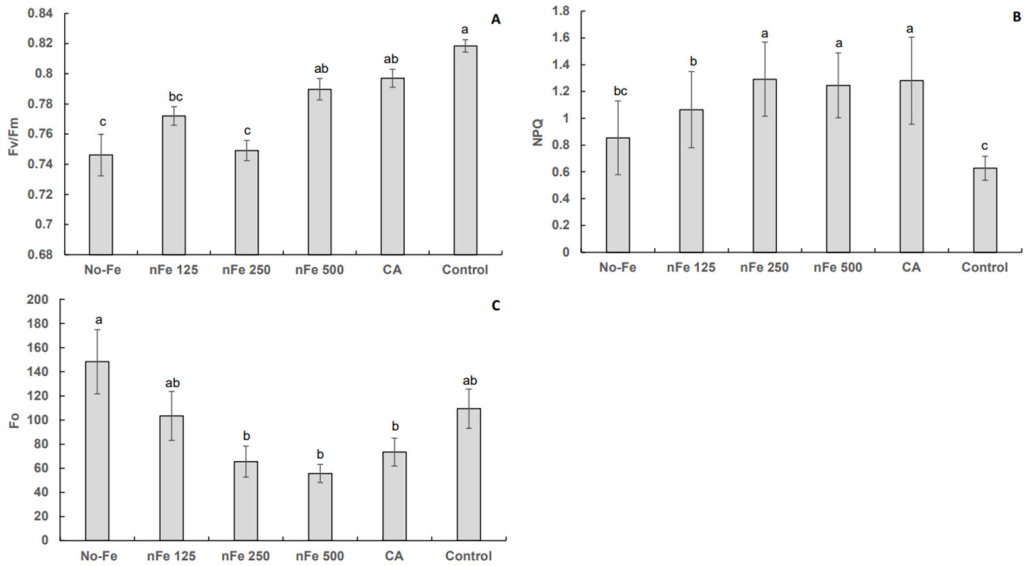

Figure 2. Maximum potential quantum efficiency of photosystem II (**A**), Non-photochemical quenching (**B**) and minimum dark-adapted fluorescence (**C**) in tomato seedlings (*Solanum lycopersicum* L. cv. 'Micro-tom') at 21 days of cultivation without iron (No-Fe); 125 mg L^{-1}, 250 mg L^{-1} and 500 mg L^{-1} of iron oxide nanoparticles (nFe 125, 250 and 500); 1.47 g L^{-1} of citric acid (CA) and Control with 1.5 mg L^{-1} FeEDTA supplied via 50% Hoagland and Arnon nutrient solution. Equal letters do not differ at the 5% probability level.

The quantum yields of photosynthesis (Fv′/Fm′) in the nFe 125, nFe 500, and CA treatments were similar to each other. On the other hand, the No-Fe and nFe 250 treatments presented reduced values (Figure 3A). The nFe 500 treatment showed higher photochemical quenching (qP) compared with the No-Fe, CA, and Control treatments (Figure 3B). At 14 DAT (days after treatment application), nFe 500 presented higher effective quantum yield of PSII (ΦPSII) than No-Fe and Control. At 21 DAT, nFe 250 and nFe 500 showed ΦPSII values similar to the Control (Figure 3C). In the iron oxide nanoparticles treatments, the electron transport rate (ETR) was higher at 14 DAT. At 21 DAT, nFe 500 maintained elevated ETR, with no significant difference from the Control (Figure 3D). At 14 DAT, heat dissipation in the antenna complex (*D*) was increased in nFe 250 and nFe 500, while the fraction of excess energy not dissipated or used in photochemistry (*Ex*) decreased. At 21 DAT, both nFe 500 and Control exhibited lower *D* values (Figure 3E). At the same time, *Ex* increased in the CA treatment (Figure 3F).

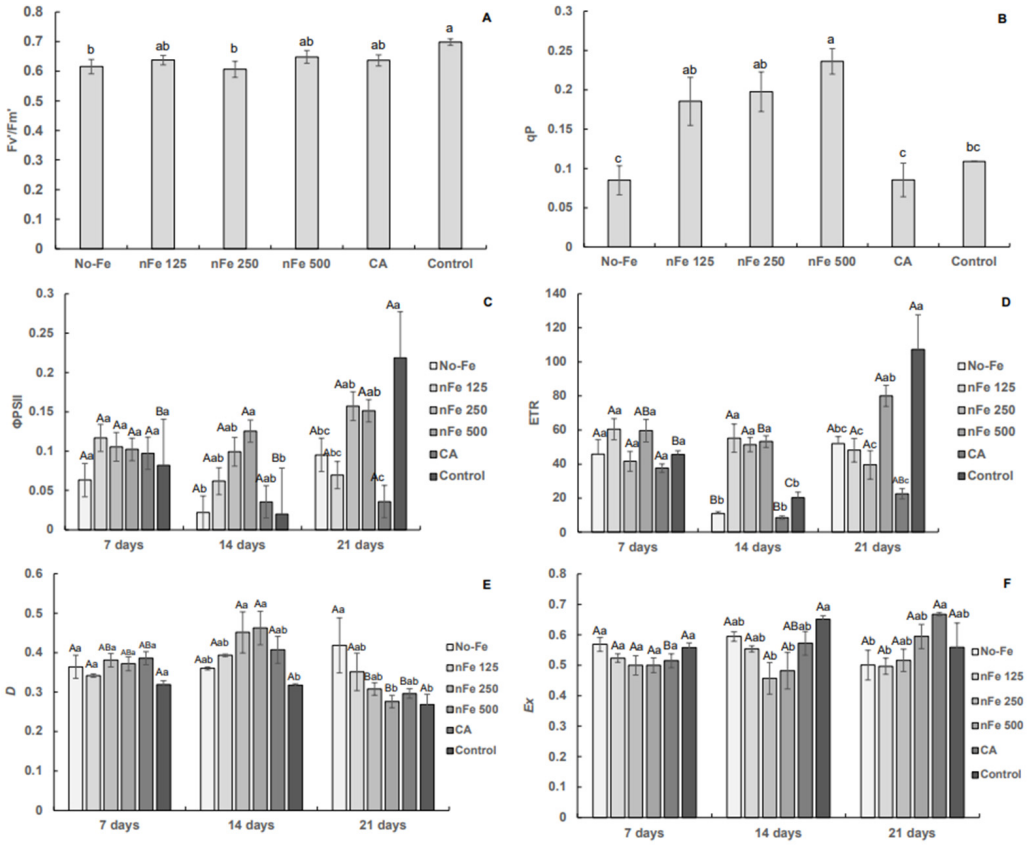

Figure 3. Effective quantum efficiency of photosystem II (**A**), Photochemical quenching (**B**), Effective quantum yield of photosystem II (**C**), Electron transport rate (**D**), Heat dissipation in the antenna complex (**E**) and Undissipated and unused energy in the photochemical phase (**F**) in tomato seedlings (*Solanum lycopersicum* L. cv. 'Micro-tom') at 21 days of cultivation without iron (No-Fe); 125 mg L^{-1}, 250 mg L^{-1} and 500 mg L^{-1} of iron oxide nanoparticles (nFe 125, 250 and 500); 1.47 g L^{-1} of citric acid (CA) and Control with 1.5 mg L^{-1} FeEDTA supplied via 50% Hoagland and Arnon nutrient solution. Equal letters do not differ at the 5% probability level. Capital letters compare evaluations within treatments and lower-case letters compare treatments within evaluations. Evaluations performed at 7, 14 and 21 days after treatment application.

3.2. Gas Exchange

At 14 DAT, CO_2 assimilation (A) in plants exposed to iron oxide nanoparticle treatments was lower than in the Control. However, at 21 DAT, nFe 500 exhibited the highest A among the nanoparticle treatments (Figure 4A). At 7 DAT, plants under nanoparticle treatments and Control displayed similar A values. At 14 DAT, transpiration rate (E) decreased in plants under nFe 500. At 21 DAT, plants under nanoparticle treatments showed E values comparable to Control (Figure 4B). Plants in the nFe 250 and nFe 500 treatments exhibited lower stomatal conductance (gs) compared with the Control at 7 DAT. At 14 and 21 DAT, gs in nanoparticle treatments did not differ significantly from the Control (Figure 4C). In nFe 125, the intercellular CO_2 concentration (C_i) at 7 and 14 DAT was higher than in nFe 500 and Control plants. At 21 DAT, plants under nFe 500 exhibited lower C_i compared with No-Fe and Control (Figure 4D). At the same time point, carboxylation efficiency (A/C_i) was higher in nFe 500 compared with all other treatments (Figure 4E). At 7 and 14 DAT, nFe 125 showed reduced instantaneous water-use efficiency (iWUE) (Figure 4F).

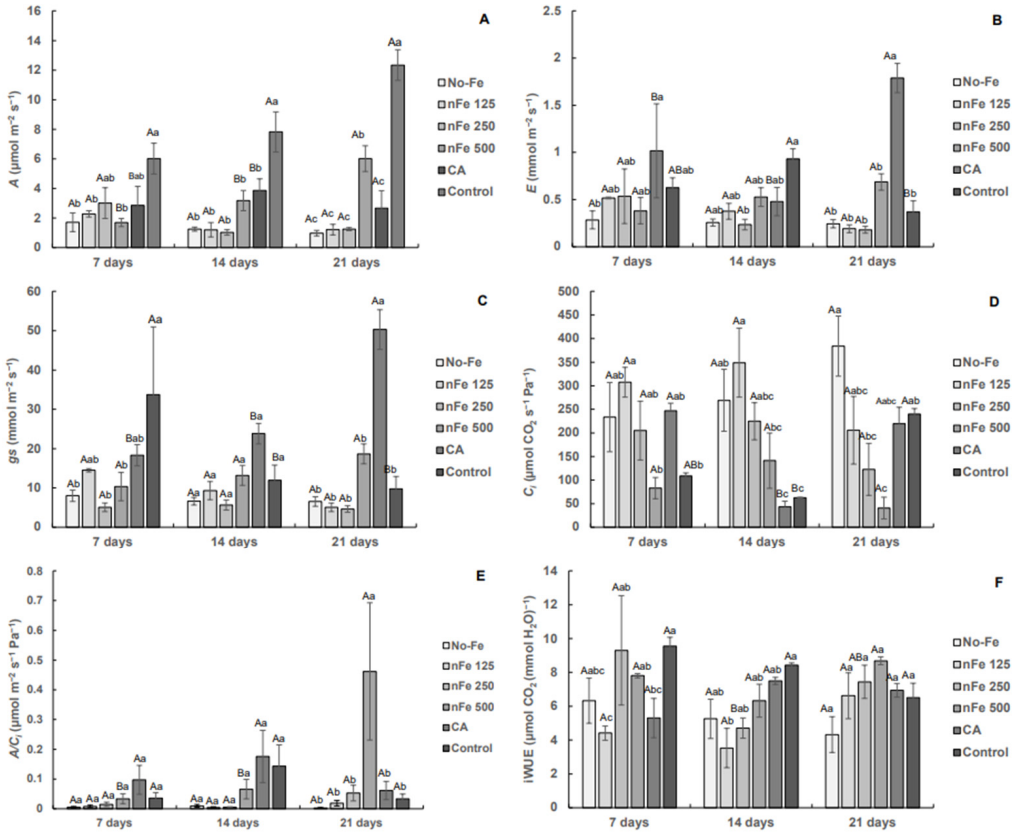

Figure 4. Net carbon assimilation (**A**), Transpiration (**B**), Stomatal conductance (**C**), Internal carbon (**D**), Instantaneous carboxylation efficiency (**E**), and Instantaneous water use efficiency (**F**) in tomato seedlings (*Solanum lycopersicum* L. cv. 'Micro-tom') at 21 days of cultivation without iron (No-Fe); 125 mg L^{-1}, 250 mg L^{-1} and 500 mg L^{-1} of iron oxide nanoparticles (nFe 125, 250 and 500); 1.47 g L^{-1} of citric acid (CA) and Control with 1.5 mg L^{-1} FeEDTA supplied via 50% Hoagland and Arnon nutrient solution. Equal letters do not differ at the 5% probability level. Capital letters compare evaluations within treatments and lower-case letters compare treatments within evaluations. Evaluations performed at 7, 14 and 21 days after treatment application.

3.3. Hydrogen Peroxide and Lipid Peroxidation

Hydrogen peroxide (H_2O_2) concentrations were higher in nFe 250 and nFe 500 compared with No-Fe, CA, and Control treatments (Figure 5A). Plants cultivated with nFe 250 exhibited greater lipid peroxidation, as indicated by higher malondialdehyde (MDA) accumulation, compared with nFe 500 and Control (Figure 5B).

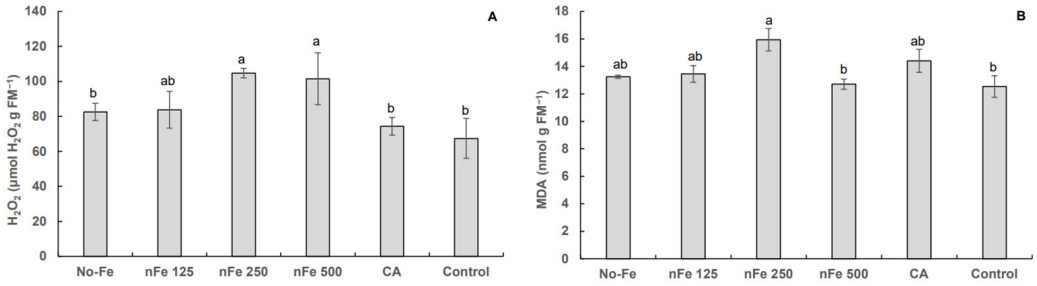

Figure 5. Quantification of hydrogen peroxide (**A**) and Malondialdehyde concentration (**B**) in tomato seedlings (*Solanum lycopersicum* L. cv. 'Micro-tom') at 21 days of cultivation without iron (No-Fe); 125 mg L^{-1}, 250 mg L^{-1} and 500 mg L^{-1} of iron oxide nanoparticles (nFe 125, 250 and 500); 1.47 g L^{-1} of citric acid (CA) and Control with 1.5 mg L^{-1} FeEDTA supplied via 50% Hoagland and Arnon nutrient solution. Equal letters do not differ at the 5% probability level.

3.4. Heatmap

The heatmap revealed the formation of two distinct clusters: Cluster I included the nFe 500, CA, and Control treatments, whereas Cluster II comprised the No-Fe, nFe 125, and nFe 250 treatments. Among the variables positively correlated with the nFe 500 treatment ($r > 0.75$) in Cluster I, the most representative were instantaneous carboxylation efficiency (A/C_i), instantaneous water use efficiency (iWUE), hydrogen peroxide (H_2O_2) concentration, photochemical quenching (qP), electron transport rate (ETR), and carbon assimilation (A). In contrast, negatively correlated variables included malondialdehyde (MDA) concentration, minimum dark-adapted fluorescence (F_0), intercellular CO_2 concentration (C_i), non-photochemical quenching (NPQ), and heat dissipation in the antenna complex (D). In the Control treatment, positive correlations were observed for ETR, effective quantum yield of PSII (ΦPSII), F_0, maximum potential quantum efficiency of PSII (Fv/Fm), effective quantum efficiency of PSII (Fv′/Fm′), and the energy neither dissipated nor used in photochemistry (Ex). The most significant negative correlations in this treatment were observed between H_2O_2 and MDA concentrations and photochemical quenching (qP). Gas exchange variables showed positive correlations with the citric acid (CA) treatment. The nFe 250 treatment, located in Cluster II, exhibited positive correlations among MDA and H_2O_2 concentrations and qP, with a notable negative correlation observed for F_0. In the No-Fe treatment, a positive correlation was observed for heat dissipation in the antenna complex (D), whereas negative correlations were associated with carbon assimilation (A), Fv/Fm, Fv′/Fm′, A/C_i, and iWUE (Figure 6).

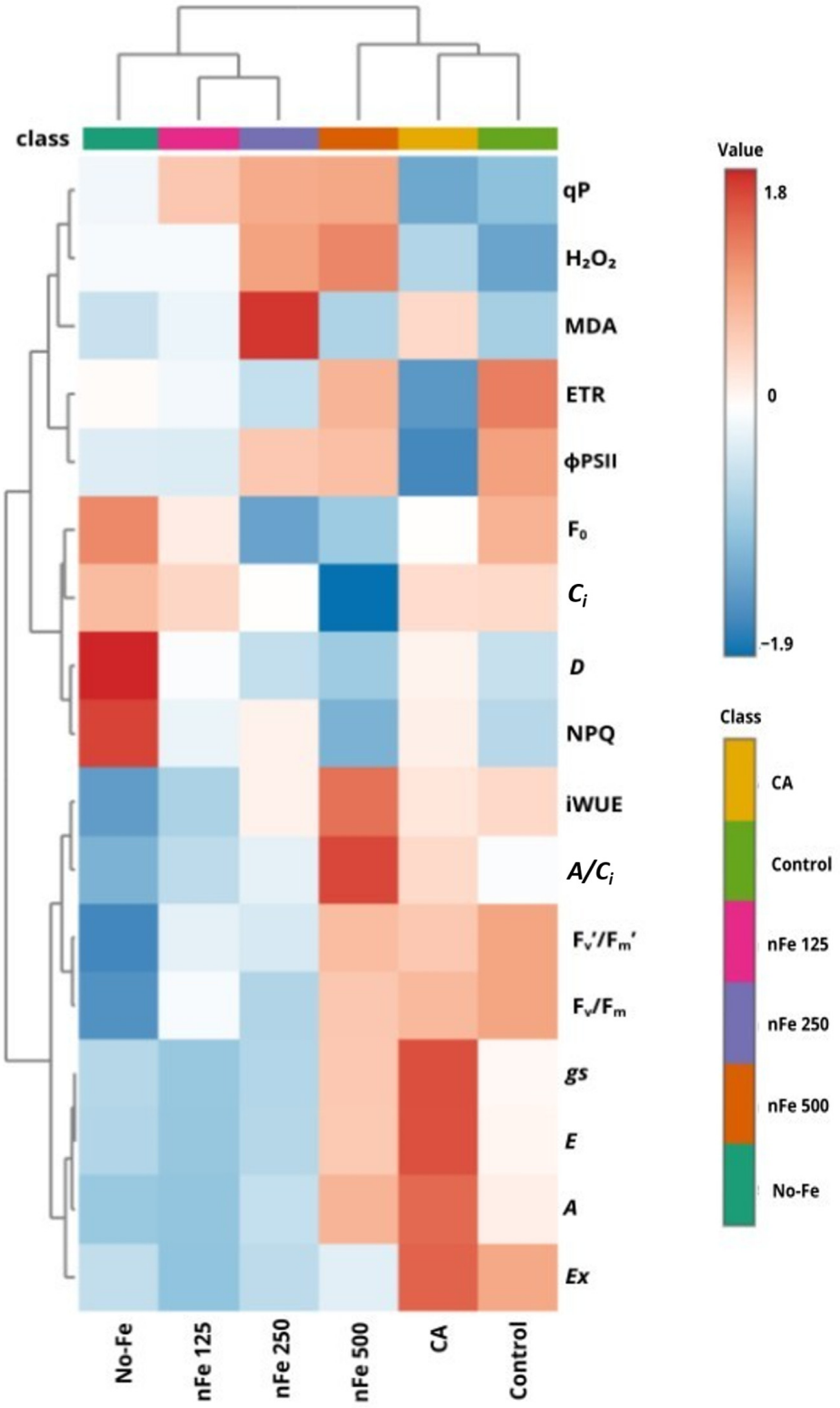

Figure 6. Heatmap and hierarchical clustering for evaluations of maximum dark-adapted fluorescence (F_m), minimum dark-adapted fluorescence (F_0), maximum potential quantum efficiency of PSII (F_v/F_m), effective quantum efficiency of PSII (F_v'/F_m'), electron transport rate (ETR), effective quantum yield of PSII (ΦPSII), photochemical quenching (qP), non-photochemical quenching (NPQ), heat dissipation in the antenna complex (*D*) and the energy not dissipated and not used in the photochemical phase (*Ex*), transpiration (*E*), stomatal conductance (*gs*), net carbon assimilation (*A*), carboxylation efficiency (A/C_i), water use efficiency (iWUE), hydrogen peroxide (H_2O_2) concentration, and malondialdehyde (MDA) concentration.

4. Discussion

Plants cultivated with nFe 500 exhibited Fv/Fm, ΦPSII, and qP values suggesting the release of Fe ions from the nanoparticles at concentrations sufficient for recovery, maintenance, and optimization of the photochemical apparatus. Furthermore, the carbon assimilation rate (*A*) was higher than in the other nanoparticle treatments, which may be attributed to the release of Fe^{3+} ions required to maintain the metabolic functions of this micronutrient. This process enabled the maintenance of electron transport and a consequent increase in NADPH + H^+ concentrations, essential for carbon reduction. This condition favored instantaneous carboxylation efficiency, as indicated by C_i and A/C_i [26].

Another relevant aspect was the stomatal opening observed in plants under the nFe 500 treatment, supported by the positive correlation of *gs* with this treatment in the heatmap. This mechanism may have favored the increase in carbon assimilation at the end of the experiment. Similar results were described by Kim et al. [27], who observed in *Arabidopsis thaliana* the activation of the *AHA2* gene, responsible for the PM H^+-ATPase proton pump, which is involved in stomatal opening. A similar phenomenon may have occurred in this study.

The high concentration of H_2O_2 observed in nFe 500 suggests that Fe ions, after being transported by the nanoparticles from roots and released into leaves, reacted with superoxide ions (O_2^-) generated during the photochemical phase of photosynthesis. This is consistent with Fenton-type reactions, in which Fe alternates its oxidation state from Fe^{2+} to Fe^{3+}, donating electrons to superoxide ions, which are rapidly protonated, resulting in H_2O_2 formation [28]. In addition, iron release by the nanoparticles may have contributed to the use of this ion as a cofactor of antioxidant enzymes such as catalase, which depends on the presence of iron in its heme group for both functionality and stability. This mechanism is directly involved in H_2O_2 decomposition and, consequently, in reducing MDA concentration [29]. It is possible that this Fenton-type reaction hypothesis in plants exposed to nFe 500 explains the maintenance of oxidative stress at low levels and the similarity to the Control treatment, suggesting that H_2O_2 may function not only as a stress indicator but also as a signaling molecule in intracellular processes.

In contrast, under nFe 250, the lower Fv/Fm indicates PSII impairment, possibly due to insufficient Fe release that could have affected the activity of essential proteins, such as iron–sulfur proteins and ferredoxin, involved in electron transport in PSII and PSI. The increase in reactive oxygen species, such as H_2O_2 and OH^-, resulting from nanoparticle application, may promote chlorophyll degradation and cleavage of the D1 protein, a PSII subunit, as previously reported [30–32]. These findings are consistent with the present study, in which higher H_2O_2 concentrations and photoinhibition (Fv/Fm) were observed. In these plants, energy dissipation as heat (NPQ) was a photoprotective strategy to minimize photochemical damage, suggesting the activation of the xanthophyll cycle [33] and maintenance of effective quantum yield of PSII (ΦPSII) at levels similar to nFe 500. The elevated H_2O_2 concentration in nFe 250 may also have stimulated molecules involved in oxidative stress signaling, such as glutathione, interfering with RuBisCO activity by altering the redox state of thiol groups, thereby inhibiting its carboxylation function. This mechanism could explain the lower carbon assimilation observed in the final evaluation [34,35]. Additionally, the higher MDA concentration may be associated with inhibition of catalase (CAT) and peroxidase (POD), possibly due to dysfunction and degradation of peroxisomes induced by oxidative stress caused by H_2O_2 accumulation in nFe 250 [36,37].

The nFe 125 treatment showed no difference in $NADPH_2$ production (ΦPSII) among treatments, and no carbon reduction was observed, as evidenced by internal carbon accumulation (C_i) and low carboxylation efficiency (A/C_i).

In the No-Fe treatment, iron deficiency appears to have impaired the function of iron–sulfur proteins in the photosystems, limiting photochemical activity and triggering photoprotective mechanisms, such as non-photochemical dissipation (observed in *D* and F_0) and the enzymatic antioxidant system. This likely reduced the plants' capacity to mitigate oxidative stress effects, possibly compromising Fe-SOD activity, one of the enzymes responsible for converting O_2^- into H_2O_2 [26,38,39], thereby explaining the low H_2O_2 accumulation.

In CA and Control, H_2O_2 presence was associated with proper antioxidant system functioning, as evidenced by low MDA concentrations.

The heatmap supported the interpretation of the most relevant variables and revealed the formation of two distinct clusters: Cluster I grouped nFe 500, CA, and Control, while Cluster II included No-Fe, nFe 125, and nFe 250. These results are consistent with the variable analyses, indicating that 500 mg L^{-1} of iron oxide nanoparticles supplied the iron demand, resembling the Control treatment.

Since nanofertilizers are characterized by their gradual release, minimizing leaching and favoring agricultural productivity, the application of 500 mg L^{-1} of iron oxide nanoparticles may represent a promising alternative as a nanofertilizer, with potential for lower environmental impact.

5. Conclusions

The application of iron oxide nanoparticles shows great potential to meet the demand for this nutrient. The positive results obtained with the nFe 500 treatment demonstrate the plants' ability to utilize Fe^{2+}/Fe^{3+} released from the nanoparticles to restore the functionality of the photosynthetic apparatus.

Supplementary Materials: The following supporting information can be downloaded at: https://www.mdpi.com/article/10.3390/environments12100346/s1: Table S1: Composition and preparation of the different nutrient solutions with or without iron oxide nanoparticles applied to *Solanum lycopersicum* L. cv. 'Micro-tom'. Table S2: Values of the least significant difference (LSD) for treatment × evaluation interaction. Table S3: Values of the least significant difference (LSD) for isolated factors (treatment and evaluation). Table S4: Values of the least significant difference (LSD).

Author Contributions: Conceptualization, J.P.S.G., F.G.C. and C.S.F.B.; methodology, J.P.S.G., F.G.C., C.d.S.R. and C.S.F.B.; validation, F.G.C., C.d.S.R. and C.S.F.B.; formal analysis, F.G.C., J.P.S.G. and C.S.F.B.; investigation, J.P.S.G., F.G.C. and C.S.F.B.; data curation, J.P.S.G., F.G.C., C.d.S.R. and C.S.F.B.; writing—original draft preparation, J.P.S.G., F.G.C. and C.S.F.B.; writing—review and editing, J.P.S.G., F.G.C. and C.S.F.B.; supervision, C.S.F.B.; project administration, F.G.C. and C.S.F.B.; funding acquisition, C.S.F.B. All authors have read and agreed to the published version of the manuscript.

Funding: National Council for Scientific and Technological Development (CNPq) for the research productivity fellowship (Process number 308038/2023-1) awarded to C.S.F. Boaro.

Data Availability Statement: This published paper includes all data produced or analyzed during this project.

Acknowledgments: Coordenação de Aperfeiçoamento de Pessoal de Nível Superior (CAPES, Brasil) supported F.G.Campos (#88881.083368/2024-01).

Conflicts of Interest: The authors declare no conflicts of interest.

References

1. Usman, M.; Farooq, M.; Wakeel, A.; Nawaz, A.; Alam Cheema, S.A.; Rehman, H.U.; Ashraf, I.; Sanaullah, M. Nanotechnology in agriculture: Current status, challenges and future opportunities. *Sci. Total Environ.* **2020**, *721*, 137778. [CrossRef]
2. Kaningini, A.G.; Nelwamondo, A.M.; Azizi, S.; Maaza, M.; Mohale, K.C. Metal nanoparticles in agriculture: A review of possible use. *Coatigns* **2022**, *12*, 1586. [CrossRef]

3. Aithal, P.S.; Aithal, S. Opportunities and challenges for green and eco-friendly nanotechnology in twenty-first century. In *Sustainable Nanotechnology: Strategies, Products, and Applications*; John Wiley & Sons: Hoboken, NJ, USA, 2022; Chapter 3, pp. 31–50. [CrossRef]
4. El-Kalliny, A.S.; Abdel-Wahed, M.S.; El-Zahhar, A.A.; Hamza, I.A.; Gad-Allah, T.A. Nanomaterials: A review of emerging contaminants with potential health or environmental impact. *Discov. Nano* **2023**, *18*, 1–21. [CrossRef] [PubMed]
5. Zheng, T.; Zhou, Q.; Tao, Z.; Ouyang, S. Magnetic iron-based nanoparticles biogeochemical behavior in soil-plant system: A critical review. *Sci. Total Environ.* **2023**, *90*, 166643. [CrossRef] [PubMed]
6. Eker, F.; Duman, H.; Akdaşçi, E.; Bolat, E.; Sarıtaş, S.; Karav, S.; Witkowska, A.M. A Comprehensive Review of Nanoparticles: From Classification to Application and Toxicity. *Molecules* **2024**, *29*, 3482. [CrossRef]
7. Paramo, L.A.; Feregrino-Pérez, A.A.; Guevara, R.; Mendoza, S.; Esquivel, K. Nanoparticles in agroindustry: Applications, toxicity, challenges, and trends. *Nanomaterials* **2020**, *10*, 1654. [CrossRef] [PubMed]
8. Wang, X.; Xie, H.; Wang, P.; Yin, H. Nanoparticles in Plants: Uptake, Transport and Physiological Activity in Leaf and Root. *Materials* **2023**, *16*, 3097. [CrossRef]
9. Van Aken, B. Gene expression changes in plants and microorganisms exposed to nanomaterials. *Curr. Opin. Biotechnol.* **2015**, *33*, 206–219. [CrossRef]
10. Tanveer, M.; Shahzad, B.; Ashraf, U. Nanoparticle application and abiotic-stress tolerance in plants. In *Plant Life Under Changing Environment: Responses and Management*; Elsevier: Amsterdam, The Netherlands, 2020; pp. 627–641. [CrossRef]
11. Mansoor, S.; Wani, O.A.; Lone, J.K.; Manhas, S.; Kour, N.; Alam, P.; Ahmad, A.; Ahmad, P. Reactive Oxygen Species in Plants: From Source to Sink. *Antioxidants* **2022**, *11*, 225. [CrossRef]
12. Movahedi, A.; Taghimolaee, M.; Ghayebpanah, S.; Monaiemi, F.; Hanbari, M.; Farahzadi, H.N. A Review of the Effect of Nanoparticles on Reactive Oxygen Species Production in Different Plants. *J. Eng. Appl. Res.* **2024**, *1*, 131–163.
13. Fang, G.D.; Zhou, D.M.; Dionysiou, D.D. Superoxide mediated production of hydroxyl radicals by magnetite nanoparticles: Demonstration in the degradation of 2-chlorobiphenyl. *J. Hazard. Mater.* **2013**, *250–251*, 68–75. [CrossRef]
14. Singh, R.P.; Handa, R.; Manchanda, G. Nanoparticles in sustainable agriculture: An emerging opportunity. *J. Control. Release* **2021**, *329*, 1234–1248. [CrossRef]
15. Yuan, J.; Chen, Y.; Li, H.; Lu, J.; Zhao, H.; Liu, M.; Nechitaylo, G.S.; Glushchenko, N.N. New insights into the cellular responses to iron nanoparticles in Capsicum annuum. *Sci. Rep.* **2018**, *8*, 3228. [CrossRef]
16. Rajput, V.; Minkina, T.; Mazarji, M.; Shende, S.; Sushkova, S.; Mandzhieva, S.; Burachevskaya, M.; Chaplygin, V.; Singh, A.; Jatav, H. Accumulation of nanoparticles in the soil-plant systems and their effects on human health. *Ann. Agric. Sci.* **2020**, *65*, 137–143. [CrossRef]
17. Yang, X.; Alidoust, D.; Wang, C. Effects of iron oxide nanoparticles on the mineral composition and growth of soybean (*Glycine max* L.) plants. *Acta Physiol. Plant* **2020**, *42*, 128. [CrossRef]
18. Hu, J.; Xianyu, Y. When nano meets plants: A review on the interplay between nanoparticles and plants. *Nano Today* **2021**, *38*, 101143. [CrossRef]
19. Martí, E.; Gisbert, C.; Bishop, G.J.; Dixon, M.S.; García-Martínez, J.L. Genetic and physiological characterization of tomato cv. *Micro-Tom. J. Exp. Bot.* **2006**, *57*, 2037–2047. [CrossRef]
20. Parrotta, L.; Aloisi, I.; Faleri, C.; Romi, M.; Del Duca, S.; Cai, G. Chronic heat stress affects the photosynthetic apparatus of *Solanum lycopersicum* L. cv Micro-Tom. *Plant Physiol. Biochem.* **2020**, *154*, 463–475. [CrossRef] [PubMed]
21. Hoagland, D.R.; Arnon, D.I. The Water-Culture Method for Growing Plants without Soil. *Calif. Agric. Exp. Stn. Circ.* **1950**, *347*, 1–32.
22. Von Caemmerer, S.; Farquhar, G.D. Some Relationships between the Biochemistry of Photosynthesis and the Gas Exchange of Leaves. *Planta* **1981**, *153*, 376–387. [CrossRef]
23. Alexieva, V.; Sergiev, I.; Mapelli, S.; Karanov, E. The effect of drought and ultraviolet radiation on growth and stress markers in pea and wheat. *Plant Cell Environ.* **2001**, *24*, 1337–1344. [CrossRef]
24. Teisseire, H.; Guy, V. Copper-Induced Changes in Antioxidant Enzymes Activities in Fronds of Duckweed (Lemna Minor). *Plant Sci.* **2000**, *153*, 65–72. [CrossRef]
25. Pang, Z.; Chong, J.; Zhou, G.; De Lima Morais, D.A.; Chang, L.; Barrette, M.; Gauthier, C.; Jacques, P.É.; Li, S.; Xia, J. MetaboAnalyst 5.0: Narrowing the Gap between Raw Spectra and Functional Insights. *Nucleic Acids Res.* 2021; 49, W388–W396.
26. Cakmak, I.; Rengel, Z.; White, P.J. Micronutrients. In *Marschner's Mineral Nutrition of Plants*; Rengel, Z., Cakmak, I., White, P.J., Eds.; Elsevier: London, UK, 2022; cap. 7; pp. 283–293.
27. Kim, J.H.; Oh, Y.; Yoon, H.; Hwang, I.; Chang, Y.S. Iron nanoparticle-induced activation of plasma membrane H+-ATPase promotes stomatal opening in Arabidopsis thaliana. *Env. Sci. Technol.* **2015**, *49*, 1113–1119. [CrossRef]
28. Smirnoff, N.; Arnaud, D. Hydrogen peroxide metabolism and functions in plants. *New Phytol.* **2019**, *221*, 1197–1214. [CrossRef]
29. Hideg, E.; Kalai, T.; Hideg, K.; Vass, I. Do oxidative stress conditions impairing photosynthesis in the light manifest as photoinhibition? In Philosophical Transactions of the Royal Society B: Biological Sciences. *R. Soc.* **2000**, *355*, 1511–1516.

30. Knaapen, A.M.; Borm, P.J.A.; Albrecht, C.; Schins, R.P.F. Inhaled particles and lung cancer. Part A: Mechanisms. *Int. J. Cancer*, 2004; 109, 799–809. [CrossRef]
31. Lu, K.; Shen, D.; Liu, X.; Dong, S.; Jing, X.; Wu, W.; Tong, Y.; Gao, S.; Mao, L. Uptake of iron oxide nanoparticles inhibits the photosynthesis of the wheat after foliar exposure. *Chemosphere* **2020**, *259*, 127445. [CrossRef] [PubMed]
32. Barzotto, G.R.; Cardoso, C.P.; Jorge, L.G.; Campos, F.G.; Boaro, C.S.F. Hydrogen peroxide signal photosynthetic acclimation of Solanum lycopersicum L. cv Micro-Tom under water deficit. *Sci. Rep.* **2023**, *13*, 13059. [CrossRef] [PubMed]
33. López-Millán, A.F.; Morales, F.; Gogorcena, Y.; Abadía, A.; Abadía, J. Metabolic responses in iron deficient tomato plants. *J. Plant Physiol.* **2009**, *166*, 375–384. [CrossRef]
34. Cohen, I.; Knopf, J.A.; Irihimovitch, V.; Shapira, M. A proposed mechanism for the inhibitory effects of oxidative stress on Rubisco assembly and its subunit expression. *Plant Physiol.* **2005**, *137*, 738–746. [CrossRef] [PubMed]
35. Hasanpour, H.; Maali-Amir, R.; Zeinali, H. Effect of TiO2 nanoparticles on metabolic limitations to photosynthesis under cold in chickpea. *Russ. J. Plant Physiol.* **2015**, *62*, 779–787. [CrossRef]
36. Hatami, M.; Ghorbanpour, M. Metal and metal oxide nanoparticles-induced reactive oxygen species: Phytotoxicity and detoxification mechanisms in plant cell. *Plant Physiol. Biochem.* **2024**, *213*, 108847. [CrossRef]
37. Abdalbagemohammedabdalsadeg, S.; Xiao, B.-L.; Ma, X.-X.; Li, Y.-Y.; Wei, J.-S.; Moosavi-Movahedi, A.A.; Yousefi, R.; Hong, J. Catalase immobilization: Current knowledge, key insights, applications, and future prospects—A review. *Int. J. Biol. Macromol.* **2024**, *276*, 133941. [CrossRef] [PubMed]
38. Melicher, P.; Dvorák, P.; Krasylenko, Y.; Shapiguzov, A.; Kangasjärvi, J.; Šamaj, J.; Takác, T. Arabidopsis Iron Superoxide Dismutase FSD1 Protects Against Methyl Viologen-Induced Oxidative Stress in a Copper-Dependent Manner. *Front. Plant Sci.* **2022**, *13*, 823561. [CrossRef] [PubMed]
39. Feng, K.; Yu, J.; Cheng, Y.; Ruan, M.; Wang, R.; Ye, Q.; Zhou, G.; Li, Z.; Yao, Z.; Yang, Y.; et al. The SOD Gene Family in Tomato: Identification, Phylogenetic Relationships, and Expression Patterns. *Front. Plant Sci.* **2016**, *7*, 1279. [CrossRef] [PubMed]

Disclaimer/Publisher's Note: The statements, opinions and data contained in all publications are solely those of the individual author(s) and contributor(s) and not of MDPI and/or the editor(s). MDPI and/or the editor(s) disclaim responsibility for any injury to people or property resulting from any ideas, methods, instructions or products referred to in the content.